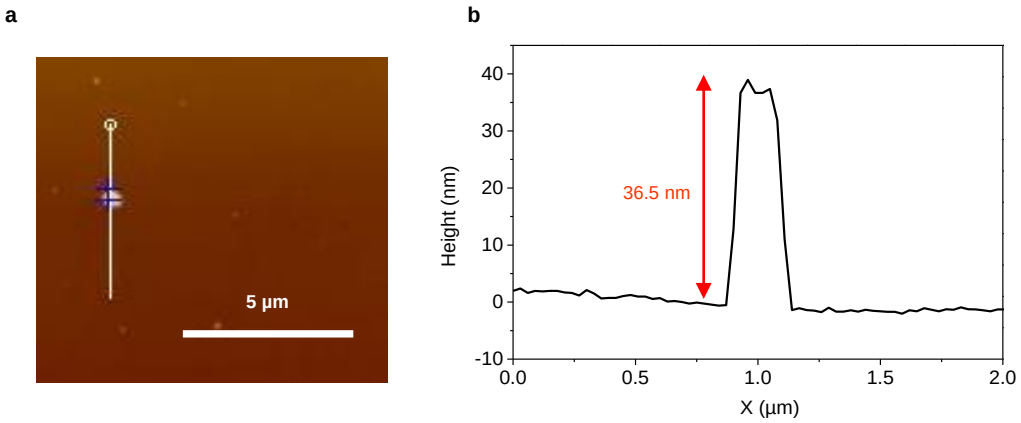

Supplementary Figure 1 | Height profile of a single Au nanodisk. (**a**) AFM image of single Au nanodisks with designed heights of h_{Ti} = 1.5 nm and h_{Au} = 35 nm. Scale bar, 5 µm. (**b**) Right: Line section of the nanodisk marked by the vertical white line in the AFM image. The measured total nanodisk thickness is in excellent agreement with the design parameters.

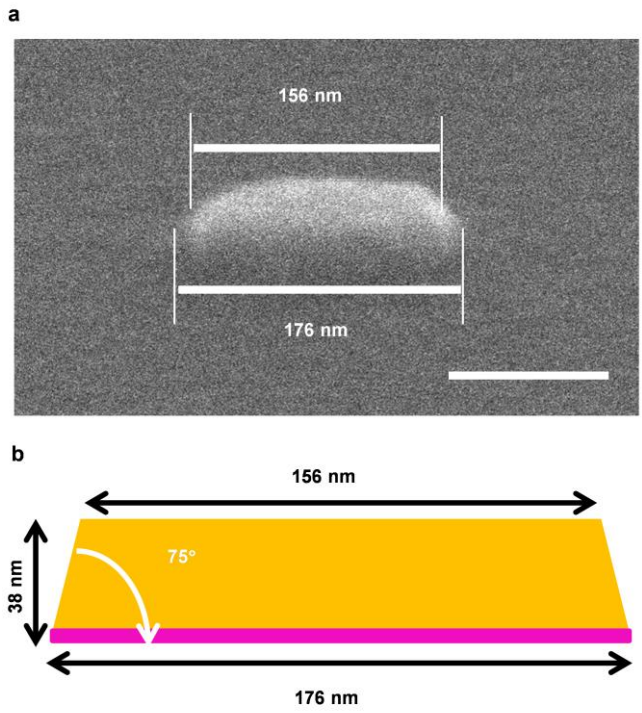

Supplementary Figure 2 | Side view of a single Au nanodisk. (**a**) SEM image of a single nanodisk. The thicknesses of the Ti and Au layers were 3 and 35 nm, respectively. The sample was mounted on a 70° tilted sample stage in order to view the cross section of the nanodisk. The bottom and top diameters of the nanodisk were measured to be 176 and 156 nm, respectively. Scale bar, 100 nm. (**b**) Diagram of the nanodisk based on the dimensions measured in (**a**). Using simple geometry, the tilt angle of the side wall was estimated to be ~ 75°.

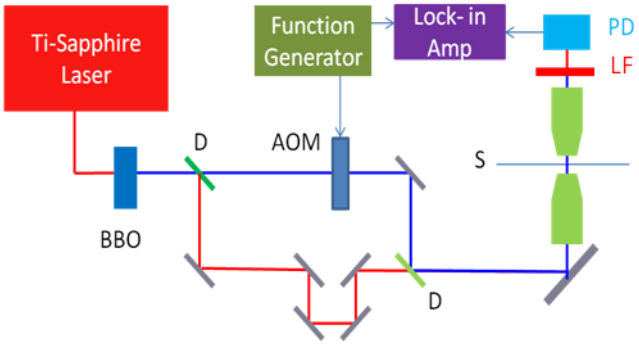

Supplementary Figure 3 | Experimental scheme of the home-built single particle transient extinction microscope. BBO: Barium boron oxide crystal; AOM: acousto-optic modulator; D: dichroic mirror; S: sample; LF: long pass filter; PD: photodiode.

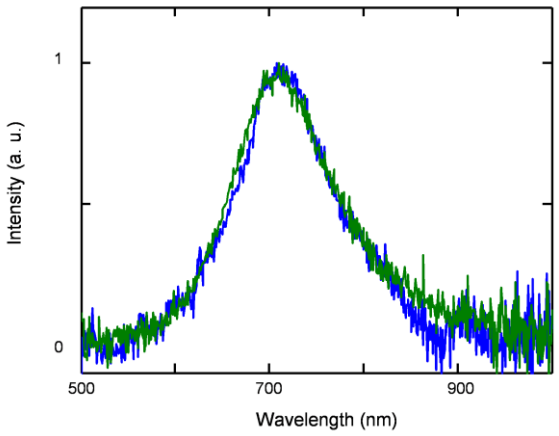

Supplementary Figure 4 | Inspection of potential laser-induced sample damage. Scattering spectra of the same nanodisk before (blue) and after (green) a transient extinction experiment. The diameter of the nanodisk was 144 nm, and h_{Ti} = 1.5 nm and h_{Au} = 35 nm. This result indicates that the nanodisk was not melted due to exposure to the femtosecond laser pulses.

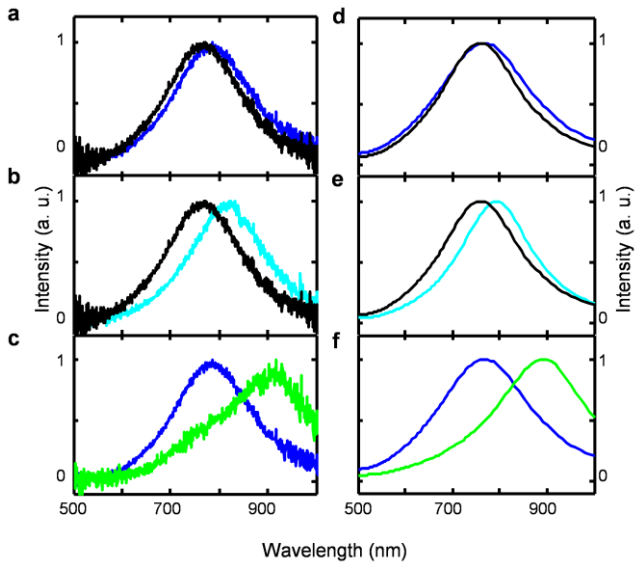

Supplementary Figure 5 | Scattering spectra of nanodisks with various Au or Ti thicknesses. Measured scattering spectra of nanodisks with (**a**) Ti thickness of 2 (blue) and 0 nm (black) where the Au thickness was 35 nm; (**b**) Au thickness of 25 (cyan) and 35 (black) nm where the Ti thickness was 0 nm; (**c**) Au thickness of 15 (green) and 35 nm (blue) where the Ti thickness was 2 nm. The diameter of these nanodisks was 176 nm. (**d**), (**e**), and (**f**) show the simulated scattering spectra assuming the same dimensions as in (**a**), (**b**), (**c**), respectively. The data shown here correspond to the samples discussed in Figures 3, and Supplementary Figures 7 and 8.

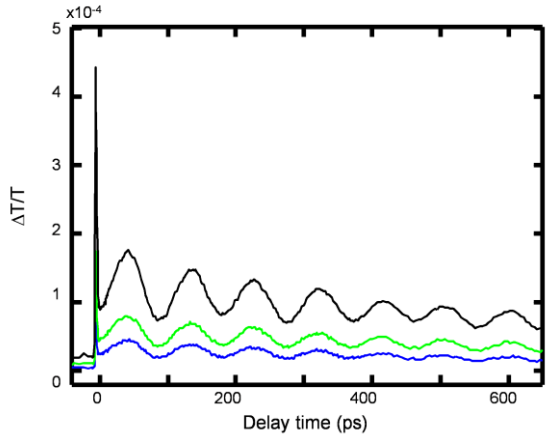

Supplementary Figure 6 | Pump power dependence of the acoustic vibration of asingle Au nanodisk. Time transient of a single nanodisk using pump powers of 33 μW (blue), 66 μW (green), and 132 μW (black). The probe power was 22 μW. The oscillation periods are the same for these traces, indicating that the frequency of the lattice vibration is independent of the pump power within the range used in this study. Using the two temperature model, the lattice temperatures for this Au/Ti nanodisk are estimated to be 349, 398, and 495 K for the pump powers used here. Temperature-induced changes of the material elastic constant due to an increased absorption by the Ti adhesion layer therefore cannot be responsible for the observed frequency shift with increasing Ti layer thickness in Figure 3. It has been reported previously that the breathing mode frequencies of Au nanospheres decrease with higher lattice temperature due to the temperature dependence of the Au elastic constants.[1] The addition of Ti increases the absorption cross section at the pump wavelength, leading to an increase of the lattice temperature for Au/Ti nanodisks with thicker adhesion layers. To estimate the difference of lattice temperatures induced by varying amount of Ti, absorption cross sections of nanodisks with 2 nm and 0 nm Ti layers were simulated, while the thickness and diameter of the Au layer was held constant at 35 and 176 nm, respectively. According to the FDTD calculations, the absorption cross sections at 410 nm are 1.92×10^4 and 1.87×10^4 nm^2 for 2 and 0 nm Ti layers. This small difference in absorption cross sections only causes a 2 K difference in the lattice temperature for a pump power of 66 μW, much smaller than the temperature variations shown here in supplementary Figure 6.

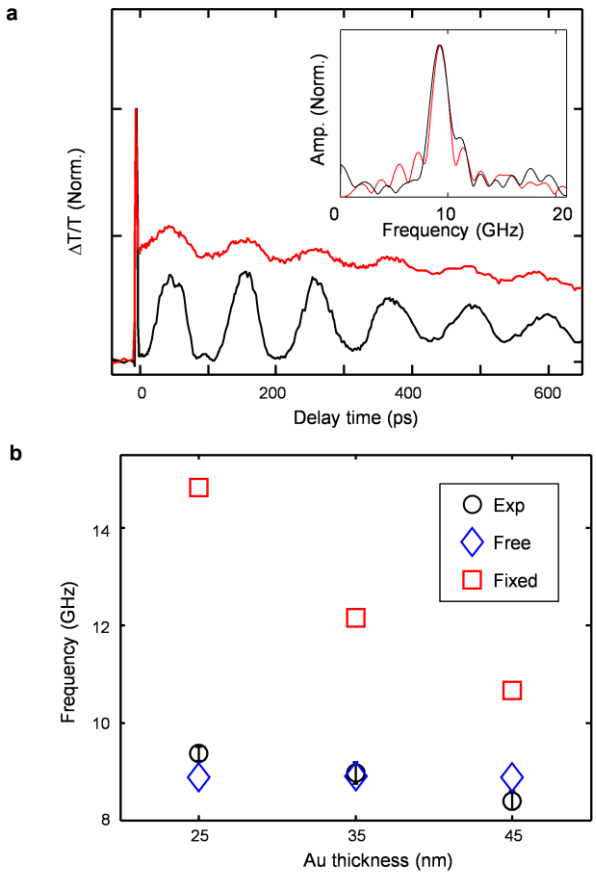

Supplementary Figure 7 | Acoustic vibrations of Au nanodisks without Ti layer. (**a**) Time transient of single nanodisks without a Ti layer and Au thickness of 25 (red) and 35 (black) nm. Inset: FT analysis with colors corresponding the time transients in the main panel. Almost identical oscillation periods were confirmed by fitting with Equation (1) (9.2 and 9.3 GHz for black and red lines, respectively) as well as FT analysis (9.2 and 9.3 GHz for black and red lines, respectively). (**b**) Experimental breathing mode frequencies (black circles) as a function of Au thickness where the Ti thickness is constant at 0 nm. FEM simulations of the breathing mode frequencies based on a free surface model (blue diamonds) and fixed surface model (red squares) are also included. The phonon frequencies redshift slightly with larger Au thickness. This trend is opposite to what is observed in Figure 3B, where the acoustic vibration frequencies blueshift with larger total thickness (Au + Ti), illustrating that the lattice vibration shift in Figure 3B is caused by the Ti layer and not by the total thickness of the nanodisk.

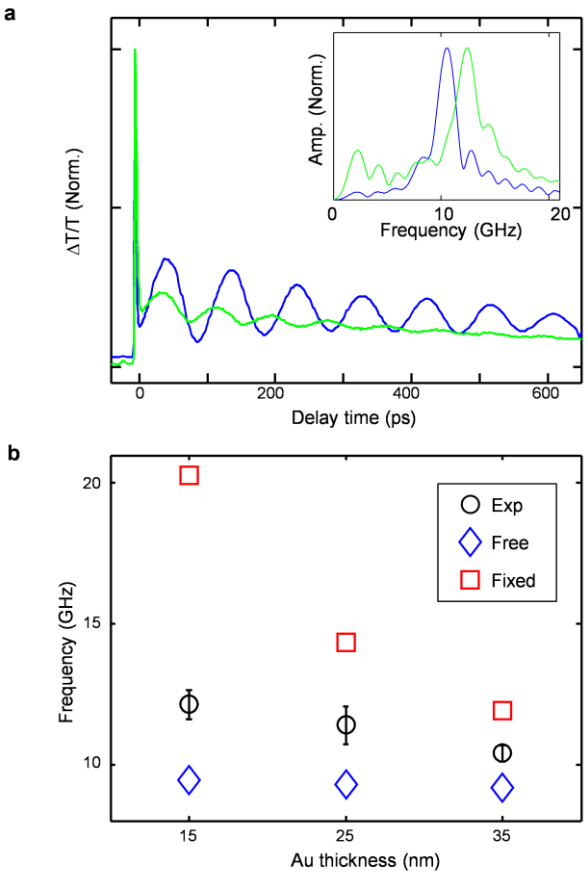

Supplementary Figure 8 | Acoustic vibrations for single nanodisks composed of various Au thicknesses and constant Ti layer height. (**a**) Time transients of single nanodisks with Au thickness of 15 (green) and 35 (blue) nm and the same Ti thickness of 2 nm. Inset: FT analysis with colors corresponding to the time transients in the main panel. The frequencies of the lattice vibrations fit with equation (1) are 10.5 GHz (blue) and 12.3 GHz (green) agree well with FT analysis (10.5 GHZ and 12.5 GHZ for blue and green curves, respectively). (**b**) Breathing mode frequencies as a function of Au thickness where the Ti thickness is constant at 2 nm. Black circles correspond to experimental data points, while the blue diamonds and red circles are obtained from FEM calculations based on a free vs. fixed surface model, respectively. The phonon frequencies redshift with larger Au thickness. This trend is stronger than without a Ti adhesion layer (Supplementary Figure 7), but still opposite to what is observed in Figure 3B, where the acoustic vibration frequencies blueshift with larger total thickness (Au + Ti), illustrating that the lattice vibration shift in Figure 3B is caused by the Ti layer and not by the total thickness of the nanodisk.

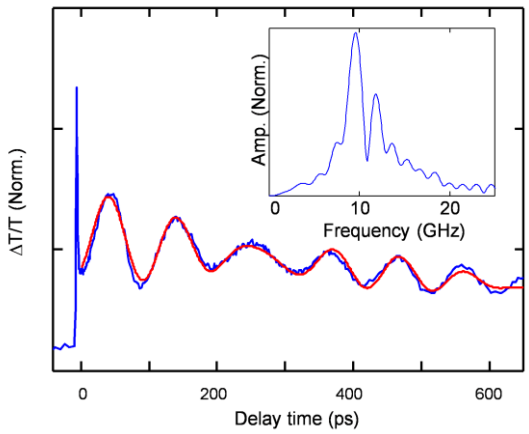

Supplementary Figure 9 | Frequency splitting due to the strong binding to the substrate. Time transient of a nanodisk with Au and Ti thicknesses of 35 and 3 nm, respectively. The red line is a fit to two oscillation frequencies. Inset: FT of the data showing two acoustic vibration frequencies.

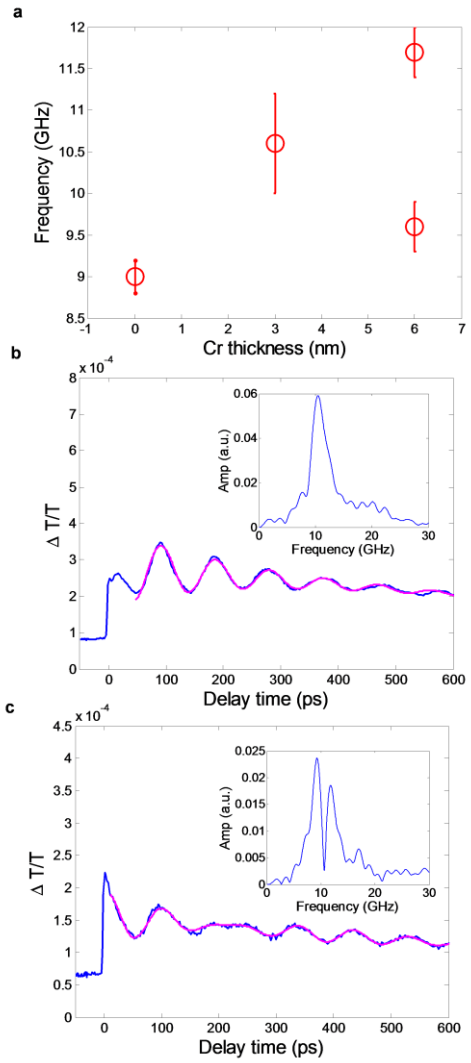

Supplementary Figure 10 | Acoustic vibrations of nanodisks with varying Cr adhesion layer thickness. (**a**) Acoustic vibration frequency as a function of Cr thickness. (**b**) Time transient of a nanodisk with Au and Cr thicknesses of 35 and 3 nm, respectively. (**c**) Time transient of a nanodisk with Au and Cr thicknesses of 35 and 6 nm, respectively. The magenta line is a fit to a single oscillation frequency for (**b**) and a fit to two oscillation frequencies for (**c**). Inset: FT of the data showing a single acoustic frequency (**b**) and two acoustic frequencies (**c**).

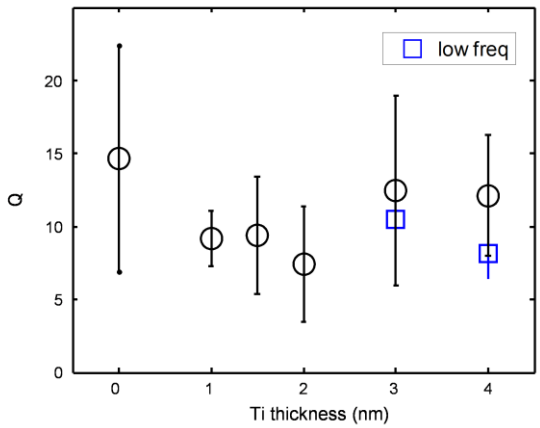

Supplementary Figure 11 | Quality factor of the nanodisk lattice vibration as a function of Ti thickness. The error bars represent the standard deviation calculated from at least 5 independent measurements on different nanodisks. The legend 'low freq' indicates values extracted from the low frequency mode.

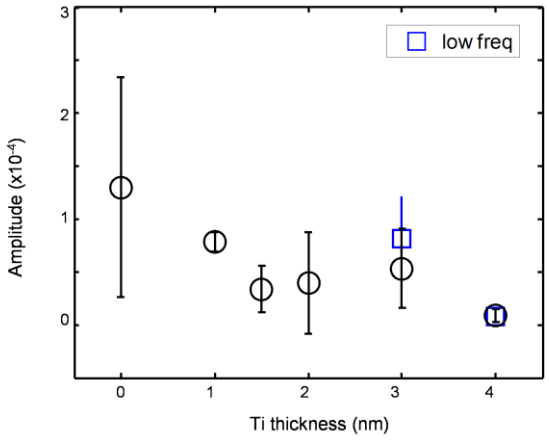

Supplementary Figure 12 | Amplitude of the damped harmonic oscillation as a function of Ti thickness. The diameter and thickness of the Au nanodisk was constant at 176 and 35 nm, respectively. The legend 'low freq' indicates values extracted from the low frequency mode.

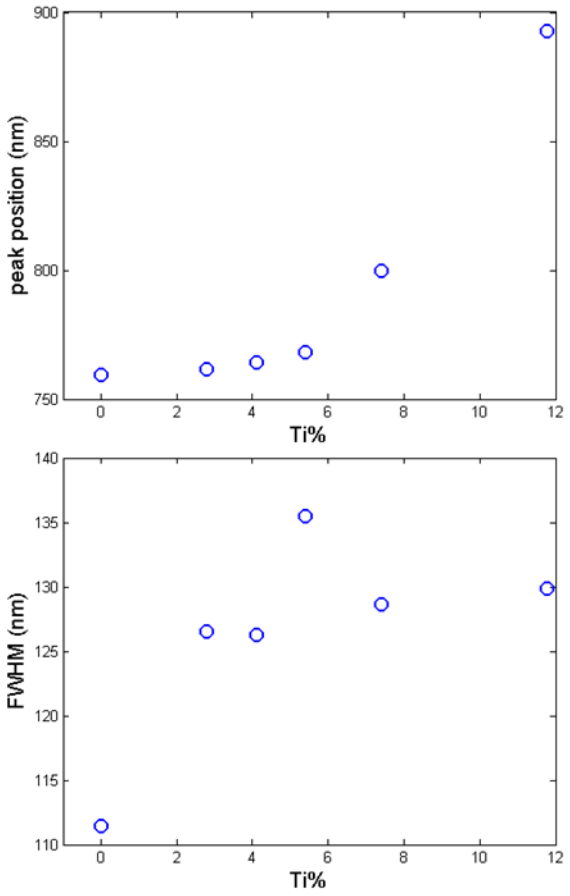

Supplementary Figure 13 | Calculated peak wavelength (top) and FWHM of Au nanodisk extinction spectra as a function of Ti %. The dimensions of the nanodisks are the same as those in Figure 4. Although the peak wavelength increases continuously (but in a non-linear behavior) as a function of Ti%, no obvious trends are observed that could be easily used to extract the Ti% of an unknown sample.

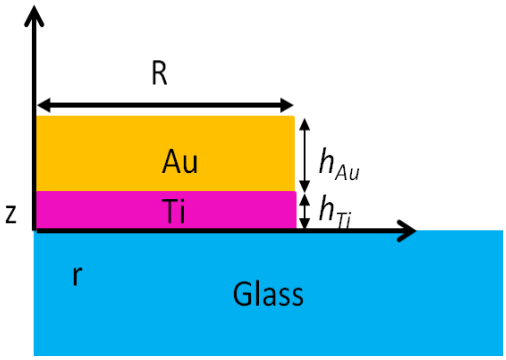

Supplementary Figure 14 | Schematic of the bimetallic nanodisk geometry that is modeled in supplementary note 2.

Supplementary Table 1 | Measured lattice vibrations of Au/Ti nanodisks with different Au and Ti thicknesses. The diameter of these disks was constant at 176 nm. The average error of the measurements for all the samples is 3.3%. Ti % is calculated according to 100 $h_{Ti}/(h_{Au}+h_{Ti})$, where h_{Ti} and h_{Au} are the height of the Ti and Au layers, respectively.

Au (nm)	15	25	25	35	35	35	35	45	35		35	
Ti (nm)	2	2	0	1	1.5	2	0	0	3		4	
Ti %	11.8	7.4	0	2.8	4.1	5.4	0	0	7.9		10.3	
Freq (GHz)	12.1	11.4	9.4	9.8	10.0	10.4	9.0	8.4	9.6	11.9	9.9	12.2
Stdev (GHz)	0.5	0.7	0.2	0.3	0.4	0.3	0.2	0.2	0.3	0.7	0.2	0.2
Error (%)	4.4	5.9	1. 6	3.2	3.7	2.8	2.5	2.3	3.1	5.9	1.5	1.2
# of disks	9	10	5	9	5	7	10	6	30		6	

Supplementary Table 2 | Summary of slopes and intercepts from Figure 2b

	slope	intercept
Fixed	0.86	7.07
Free	1.54	0.35
Analyt	1.79	-0.78
Exp	1.90	-0.55

Supplementary Table 3 | Summary of slopes and intercepts from Figure 3b

	slope	intercept
Fixed	-0.12	12.16
Free	0.13	8.92

Supplementary Note 1: Breathing and extensional modes

In general, only the radial breathing modes of disk-shaped nanoparticles are observed experimentally in the limiting case of large aspect ratio *D*/*h* where *h* is the thickness and *D* is the diameter.[2-4] The ratio of the resonant frequencies for the fundamental breathing and extensional modes for a free disk is a function of the disk aspect ratio and can be expressed as follows:

$$\frac{\omega_{\mathrm{br}}}{\omega_{\mathrm{ext}}} = \frac{h}{R}\frac{\tau_n}{(2n-1)\pi}\sqrt{\frac{(1-2\sigma)}{(1-\sigma)^2}}, \qquad \text{(Supplementary Equation 1)}$$

where the subscripts "ext" and "br" refer to the extensional and breathing modes, respectively, ω is the radial frequency, R is the radius, σ is the Poisson ratio of the solid, and τ_n is a parameter given by

$$\tau\, J_0(\tau) = (1-\sigma)\, J_1(\tau)\,. \qquad \text{(Supplementary Equation 2)}$$

Supplementary Note 2: Analytical model for breathing mode vibration of a free bimetallic disk

We consider a free axisymmetric bimetallic disk that is undergoing breathing mode oscillations along its radius, i.e. without the glass substrate in Supplementary Figure 14. As the amplitude of the oscillation is far smaller than any other geometric length scale of the particle, the solid particle is assumed to obey the linear elastic theory. The corresponding equation for the solid is the Navier's equation:[5]

$$\rho_{\mathrm{s}}\frac{\partial^2 \mathbf{u}}{\partial t^2} = \frac{E}{2(1+\sigma)}\left\{\boldsymbol{\nabla}^2\mathbf{u} + \frac{1}{(1-2\sigma)}\boldsymbol{\nabla}\left(\boldsymbol{\nabla}\cdot\mathbf{u}\right)\right\}, \qquad \text{(Supplementary Equation 3)}$$

where $\boldsymbol{u}$ is the solid displacement field, ρ_{s} is the solid density, and E is Young's modulus. As the motion is oscillatory, the time-dependent solid displacement can be expressed in terms of the explicit time dependence, $e^{-i\omega t}$:

$$\mathbf{u}(r,z,t) = \tilde{\mathbf{u}}(r,z\,|\omega)\, e^{-i\omega t}, \qquad \text{(Supplementary Equation 4)}$$

where ω is the radial frequency, t is time, and i is the usual imaginary unit. For simplicity, we henceforth omit the superfluous '~' notation, noting that the above relation holds universally.

The analytical theory has been developed considering the limit where one of the geometric length scales, *h*, is much smaller than the other geometric length scale, *R*. In this limiting case, breathing modes exhibit a pure radial displacement, i.e., $\mathbf{u}_{\mathrm{br}}(\boldsymbol{r}) = u_{\mathrm{br}}(r)\hat{\mathbf{r}}$. Therefore, the governing equation for the radial displacement is:

$$\frac{\mathrm{d}^2 u_{\mathrm{br}}}{\mathrm{d}r^2} + \frac{1}{r}\frac{\mathrm{d}u_{\mathrm{br}}}{\mathrm{d}r} - \frac{u_{\mathrm{br}}}{r^2} + \tau^2\, u_{\mathrm{br}} = 0, \qquad \text{(Supplementary Equation 5)}$$

where $\tau^2 = R^2\omega_{\mathrm{br}}^2(h_{\mathrm{Au}}\rho_{\mathrm{Au}} + h_{\mathrm{Ti}}\rho_{\mathrm{Ti}})/(\alpha_{\mathrm{Au}} + \alpha_{\mathrm{Ti}})$, $\alpha_{\mathrm{Au}} = h_{\mathrm{Au}}\, E_{\mathrm{Au}}/(1-\sigma_{\mathrm{Au}}^2)$, and $\alpha_{\mathrm{Ti}} = h_{\mathrm{Ti}}\, E_{\mathrm{Ti}}/(1-\sigma_{\mathrm{Ti}}^2)$. The subscripts Au and Ti indicate values for gold and titanium, respectively. We assume finite displacement at the center of the particle, matching the displacement at the solid-solid interface and zero normal force conditions at the disk free surface. Solving Supplementary Equation 5 together with the boundary condition then provides the expression for the radial displacement:

$$u_{\mathrm{br}}(r) = \frac{J_1\left(\tau\frac{r}{R}\right)}{J_1(\tau)}. \qquad \text{(Supplementary Equation 6)}$$

The parameter τ in Supplementary Equation 6 is specified by the eigenvalue equation:

$$\tau\, J_0(\tau) = \frac{(1-\sigma_{\mathrm{Au}})\alpha_{\mathrm{Au}} + (1-\sigma_{\mathrm{Ti}})\alpha_{\mathrm{Ti}}}{\alpha_{\mathrm{Au}} + \alpha_{\mathrm{Ti}}}\, J_1(\tau). \qquad \text{(Supplementary Equation 7)}$$

The resonant frequencies are given by:

$$\omega_{\mathrm{br}}^{(n)} = \frac{\tau_n}{R}\sqrt{\frac{(\alpha_{\mathrm{Au}} + \alpha_{\mathrm{Ti}})}{(h_{\mathrm{Au}}\rho_{\mathrm{Au}} + h_{\mathrm{Ti}}\rho_{\mathrm{Ti}})}}. \qquad \text{(Supplementary Equation 8)}$$

In the above equation $\tau_n$is the *n*-th root of Supplementary Equation 7.

In order to consider the tilt angle of the sidewalls of the disk in the analytical model (Supplementary Figure 2), we have calculated the acoustic frequencies using the average of the bottom and top diameters of the nanodisk.

Supplementary Note 3: Calculation of electron and lattice temperatures by the two temperature model

We estimated the highest lattice temperature of the nanodisks induced by the femtosecond pump pulse using the two-temperature model.[6] Our assumptions are as follows: (1) all absorbed energy heats the electrons; (2) no energy dissipates into the environment during this process; (3) the pump laser pulse is treated as a delta function, so the pulse does not affect the

system after initial heating the electrons; (4) the heat capacity of the lattice is independent of temperature; (5) the heat capacity and density of gold are taken from bulk gold data. (6) hot electron diffusion within the Au disk and at the Au - Ti interface are ignored.[7] The latter assumption is expected to yield a slight overestimation of the electron and lattice temperatures. For a gold nanodisk with a diameter of 176 nm and a thickness of 35 nm, the calculated absorption cross section at 410 nm is 1.86×10^{-14} m^2. After the gold nanodisk is illuminated by the pump laser pulse with an energy density per pulse of 10.97 Jm^{-2}(heating power: 66 μW, beam radius: 150 nm), the electron temperature T_e reaches 2,612 K for a heat capacity of $C_e(T_e) = A_e T_e$, where A_e is 71 $Jm^{-3}K^{-2}$.[8] Then the temperatures of the electrons and lattice T_L as a function of time are described by the two-temperature model according to:[6]

$$\frac{\partial(C_e T_e)}{\partial t} = -g(T_e - T_L) \qquad \text{(Supplementary Equation 9)}$$

$$\frac{\partial(C_L T_L)}{\partial t} = g(T_e - T_L) \qquad \text{(Supplementary Equation 10)}$$

where C_L is the heat capacity of bulk gold and g is 2.1×10^{16} $Wm^{-3}K^{-1}$ for gold.[8] At equilibrium, the maximum T_L is 396 K, which is much lower than the melting point of bulk gold. To estimate the highest lattice temperature of a bimetallic nanodisk with a diameter of 176 nm and 35 nm thick Au and 2 nm thick Ti layers, we further assumed that all of the energy absorbed is used to heat the electrons and lattice of the gold, yielding an upper bound. The calculated absorption cross section of the bimetallic nanodisk at 410 nm is 1.89×10^{-14} m^2. The initial temperature of the electrons is then 2,640 K, and the highest temperature of the lattice is 398 K, which is also lower than the melting point of bulk gold. These estimations confirm that our samples did not melt during the transient extinction measurements. In addition, the presence of Ti only increases the lattice temperature from 396 to 398 K with excitation power of 66 μW at 410 nm.

Supplementary Note 4: Height dependence of the nanodisk breathing frequency for free and fixed surface models

To investigate the effect of total nanodisk height on the breathing mode frequency, we investigated nanodisks with varying height and 0 nm Ti layer (Supplementary Figure 7) and 2 nm Ti layer (Supplementary Figure 8). Experimental time transients are shown for sample nanodisk structures in Supplementary Figures 7A and 8A. Supplementary Figure 7B illustrates breathing mode frequencies of nanodisks with Au thickness of 25, 35, and 45 nm in the absence of a Ti layer. The experimental results (black circles) agree well with the free surface model (blue diamonds); the breathing mode frequencies slightly decrease with Au thickness, despite the

analytical model's predictions (Supplementary Equation 8) that the frequencies are independent of the height. Because of the absence of a Ti layer, this frequency shift with Au thickness is a purely intrinsic effect of the material. It is known that Au possesses a high Poisson coefficient, which measures the negative ratio of axial to radial strain. A pure thickness independent breathing mode can only be observed when the disk is much thinner than in the present case (thickness/diameter < 0.1).

In comparison, the fixed surface model (red squares in Supplementary Figure 7B) predicts a more significant thickness dependence of the breathing mode frequencies. Although the fixed surface model is not realistic for a nanodisk without a Ti layer, this trend can be explained qualitatively by the elastic model. The resonant frequency of a mechanical system depends on its stiffness. When the bottom surface of the disk is fixed, its movement is restrained in the radial direction. This increases the stiffness of the disk, which enhances its resonant frequency. Increasing the disk thickness reduces the effect of this restraint, thus reducing the disk stiffness and resonant frequency.

To confirm the thickness dependence on the breathing mode frequencies for the case that is more adequately described by the fixed surface model, nanodisks with a 2 nm Ti adhesion layer and Au layers of 15, 25 and 35 nm were fabricated and investigated optically (Supplementary Figure 8). The breathing mode frequencies indeed increase more drastically for nanodisks with a thinner Au thickness for a 2 nm Ti adhesion layer (Supplementary Figure 8B). The experimental results (black circles) show a significant decrease of the breathing mode frequency with larger Au thickness, and are consistent with the fixed surface model despite the smaller slope considering that for a 2 nm adhesion layer the nanodisks are not completely bound to the surface (Figure 3B).

Supplementary References:

1 Hartland, G. V., Hu, M. & Sader, J. E. Softening of the Symmetric Breathing Mode in Gold Particles by Laser-Induced Heating. *J. Phys. Chem. B* **107**, 7472-7478, (2003).

2 Hu, M. *et al.* Vibrational Response of Nanorods to Ultrafast Laser Induced Heating: Theoretical and Experimental Analysis. *J. Am. Chem. Soc.* **125**, 14925-14933, (2003).

3 Petrova, H. *et al.* Time-resolved spectroscopy of silver nanocubes: Observation and assignment of coherently excited vibrational modes. *J. Chem. Phys.* **126**, 094709, (2007).

4 Petrova, H. *et al.* Vibrational Response of Au−Ag Nanoboxes and Nanocages to Ultrafast Laser-Induced Heating. *Nano Lett.* **7**, 1059-1063, (2007).

5 Landou, L. D. & Lifshitz, E. M. *Theory of Elasticity. 3rd ed.*, (Butterworth-Heinemann, 1986).

6 Del Fatti, N. *et al.* Nonequilibrium electron dynamics in noble metals. *Phys. Rev. B* **61**, 16956-16966, (2000).

7 Eschenlohr, A. *et al.* Ultrafast spin transport as key to femtosecond demagnetization. *Nat. Mater.* **12**, 332-336, (2013).

8 Hohlfeld, J. *et al.* Electron and lattice dynamics following optical excitation of metals. *Chem. Phys.* **251**, 237-258, (2000).